Tunneling anisotropic magnetoresistance on the atomic scale

K. von Bergmann,[1,*] M. Menzel,[1] D. Serrate,[1] Y. Yoshida,[1] S. Schröder,[2] P. Ferriani,[2] A. Kubetzka,[1] R. Wiesendanger,[1] and S. Heinze[2]

[1]*Institut für Angewandte Physik, Universität Hamburg, Jungiusstr. 11, 20255 Hamburg, Germany*

[2]*Institut für Theoretische Physik und Astrophysik, Christian-Albrecht-Universität zu Kiel, Leibnizstr. 15, 24098 Kiel, Germany*

(Received 11 April 2012; published 24 October 2012)

We demonstrate the occurrence of tunneling anisotropic magnetoresistance on the atomic scale using scanning tunneling microscopy (STM). Our experiments show that noncollinear atomic-scale magnetic structures can be revealed in STM using nonmagnetic tips. These observations can be explained by a variation of the local density of states of an atom depending on its magnetization direction due to spin-orbit interaction. STM simulations based on this effect are in excellent agreement with the experimental images and can explain the bias-voltage-dependent contrast found for two-dimensionally modulated spin textures.

DOI: 10.1103/PhysRevB.86.134422 PACS number(s): 75.70.Tj, 68.37.Ef, 75.25.−j

One of the driving forces in the field of spintronics is the promise to realize low-dissipative devices combining the ability to store and process information which could replace current microelectronics. In this respect, observation of the tunneling anisotropic magnetoresistance (TAMR) effect in planar junctions[1] triggered great research activity since it requires only one ferromagnetic electrode and allows integration with semiconductor interfaces. Following the first report of TAMR in a planar tunnel junction consisting of a magnetic semiconductor, an oxide spacer, and a metallic layer, the effect was also demonstrated for semiconducting spacers,[2] as well as antiferromagnetic[3] and organic spin valves.[4] Recently, top-down approaches were used to demonstrate domain sensing on the submicron scale via TAMR[5] and a ferromagnetic-semiconductor-based read-write device was designed employing the TAMR to read out the information.[6] Theoretical studies even proposed the occurrence of TAMR in nanocontacts and break junctions[7,8] and experimental evidence was reported for the latter.[9,10] The detection of TAMR on the atomic scale for single Mn atoms embedded in GaAs using scanning tunneling microscopy (STM)[11] was also predicted, however, experimental proof is lacking. Interestingly, prior to the studies in planar tunnel junctions, the TAMR effect had already been used in STM experiments to resolve nanometer-scale domain walls in ultrathin ferromagnetic films.[12]

The origin of TAMR for planar tunnel junctions is well established as a magnetization-direction-dependent change of the band structure due to spin-orbit coupling (SOC).[1,12–14] Typically the angular dependence of TAMR is measured by rotating an external magnetic field, which either continuously rotates the magnetic layer or leads to defined switching events. In view of future device miniaturization it is essential to seek the limiting structure size, i.e., whether TAMR can also be observed on the atomic scale, when the magnetization direction changes from atom to atom. In order to study this ultimate limit it is practical not to use external magnetic fields but, instead, to choose systems which intrinsically have a varying magnetization direction, i.e., noncollinear magnetic structures.

Here, we apply STM to demonstrate the possibility of observing and using the TAMR effect on the atomic scale, focusing on three model systems with atomic-scale noncollinear magnetic ground states. We introduce a model for the tunnel current based on the spatial variation of the local density of states (LDOS) due to SOC. Our simulations of STM images allow us to understand the observed patterns as well as the bias voltage dependence for a two-dimensionally modulated spin structure.

We consider noncollinear magnetic structures at surfaces in which the magnetization direction varies from atom to atom. Let us assume for simplicity that the magnetic moment is constant in value and that all atom sites are equivalent as long as we neglect SOC. We can define a local spin quantization axis at each atom α by the angles $(\phi_\alpha,\theta_\alpha)$ in spherical coordinates and express the wave function of band ν and Bloch vector $\mathbf{k}$ locally in a spin-up $\psi^{\uparrow}_{\nu\mathbf{k}}$ and a spin-down $\psi^{\downarrow}_{\nu\mathbf{k}}$ part. Since SOC is a small effect, it can be treated in a perturbative way, and to first order we obtain a change $\delta\psi_{\nu\mathbf{k}}$ in the wave function $\psi_{\nu\mathbf{k}}$ which scales with the SOC matrix element $\langle\psi^{\sigma'}_{\mu\mathbf{k}}|H_{\mathrm{SO}}|\psi^{\sigma}_{\nu\mathbf{k}}\rangle$. The matrix element mixes states of different spin and orbital characters and its angular dependence is given by $\langle\psi^{\sigma'}_{\mu\mathbf{k}}|\mathbf{ls}|\psi^{\sigma}_{\nu\mathbf{k}}\rangle$. As a consequence, the LDOS of atom α contains a term which depends on the direction of its magnetic moment, i.e., $n_\alpha = n^o_\alpha + \Delta n_\alpha(\phi_\alpha,\theta_\alpha)$.

We can incorporate this effect within the independent orbital approximation of the tunnel current,[15,16]

$$I(\mathbf{R}_T) \propto \sum_\alpha \left(1 + P_T P_S \cos\delta_\alpha + \frac{\Delta n_\alpha}{n^o_\alpha}\right) h(\mathbf{R}_T - \mathbf{R}_\alpha), \qquad (1)$$

where $\mathbf{R}_T$ is the tip position, the sum extends over all atoms α, $h(\mathbf{r}) = \exp(-2\kappa|\mathbf{r}|)$, and the decay constant is $\kappa = \sqrt{2m\phi/\hbar^2}$ with the work function ϕ. P_S and P_T denote the spin polarization of sample and tip atoms, respectively, and δ_α is the angle between the magnetization of atom α and the tip magnetization direction $\mathbf{m}_T$. The three contributions to the current represent the atomic corrugation, the spin-polarized part, and the TAMR effect.

The tunnel current and the STM image are dominated by states which decay most slowly into the vacuum. Therefore, the variation of the LDOS depends on the orbital and spin character of the band ν with the highest vacuum contribution, e.g., being of d_{z^2} character, and of the band μ it is mixing with. The angular dependence of the matrix element can be expressed via a function $f(\phi_\alpha,\theta_\alpha)$ based on the SOC matrix elements.[17] We then obtain for the change in the LDOS $n_\alpha = n^0_\alpha(1 + \gamma f(\phi_\alpha,\theta_\alpha))$, where $\gamma = \Delta n/n_o$ is a constant denoting

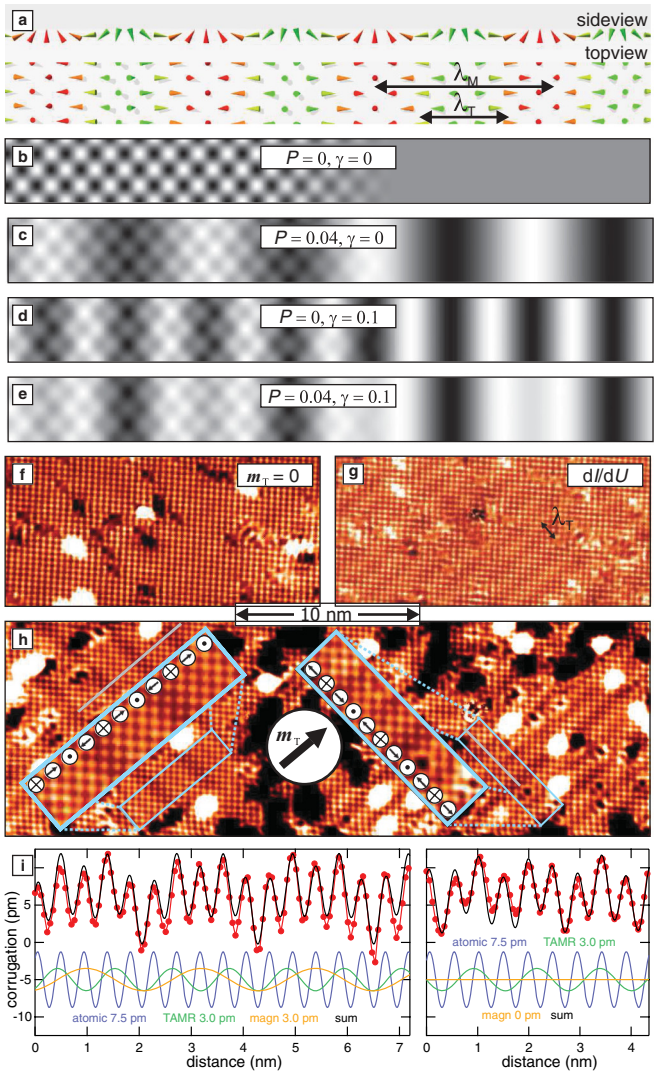

FIG. 1. (Color online) Simulated and measured (spin-polarized) STM images of the Mn monolayer on W(001).[19] (a) Sketch of the spin spiral. (b–e), Simulated STM images of this spin structure for a tip-sample distance of 5 Å (left) and 10 Å (right) for different P and γ values. (f) Non-spin-polarized STM image (W tip) with atomic resolution and a weak TAMR signal and (g) simultaneously obtained $\mathrm{d}I/\mathrm{d}U$ map. (h) Spin-polarized STM image (Fe-coated W tip; $\mathbf{m}_\mathrm{T}$ indicated by arrow) with the two possible rotational domains. Insets: Magnified views of the image indicating the spin spiral. (i) Height profiles [top (red) line with circles] along the solid (gray) lines indicated in (h) and their decomposition into atomic, TAMR, and magnetic contributions. All: $I = 1$ nA, $U = +50$ mV, $T = 13$ K.

the integrated LDOS change over energy up to the applied bias voltage.[18] Ideal systems for observation of the TAMR on the atomic scale are surfaces with a spin spiral ground state, as all atom sites are electronically equivalent without SOC and any LDOS modulation can be unambiguously related to SOC.

Figure 1(a) displays a sketch of a planar cycloidal spin spiral propagating along the [110] direction of a bcc-(001) surface. Simulated STM images of this structure [Fig. 1(b)] display the atomic sites if we assume a non-spin-polarized tip (effective polarization $P = P_T P_S = 0$) and neglect the TAMR ($\gamma = 0$). At larger separation the atomic resolution is lost [Fig. 1(b), right]. As the spin-polarized part of the tunnel current depends on P and $\cos\delta_\alpha$ [cf. Eq. (1)], an STM measurement with a magnetic tip will result in a stripe pattern with the magnetic period λ_M [Fig. 1(c)]. For a planar spin spiral, the LDOS modulation due to SOC is given by $f(\phi_\alpha,\theta_\alpha) = \cos^2\theta_\alpha$ if only states of the same spin channel mix at the Fermi level due to a large exchange splitting of majority and minority bands.[20] Therefore, the simulated STM image due to the TAMR is a stripe pattern with a period of $\lambda_T = \lambda_M/2$ [Fig. 1(d)]. In an experiment with a magnetic tip both the spin-polarized and the TAMR contribution to the tunnel current can coexist, which leads to an STM image as in Fig. 1(e).

Figures 1(f)–1(h) display STM measurements of the Mn monolayer on the W(001) surface. The magnetic ground state of this system is a planar cycloidal spin spiral with a period of $\lambda_M \approx 2.4$ nm[19] [Fig. 1(a)]. The STM image in Fig. 1(f) shows a typical surface area with atomic resolution measured with a nonmagnetic W tip. Since the huge atomic corrugation of 13 pm dominates the STM image, the signal due to TAMR (1 pm) is only barely visible. However, in the simultaneously acquired $\mathrm{d}I/\mathrm{d}U$ map [Fig. 1(g)], a small but distinct modulation due to the TAMR with a wavelength of $\lambda_T \approx 1.2$ nm, i.e., $\lambda_M/2$, clearly shows up, which is in good agreement with the simulation shown in Fig. 1(d).

Figure 1(h) displays a spin-polarized STM image with the two possible rotational domains,[19] i.e. the tunnel current consists of all three parts displayed in Eq. (1) [cf. line profiles in Fig 1(i)]. While the left domain shows a magnetic corrugation of 3 pm, the other rotational domain does not possess a clear sign of magnetic contrast. The different appearance of the two domains must be due to the cosine-dependence of the spin-polarized tunnel current, since the TAMR effect and the atomic signal are the same for both cases. From this we infer a tip magnetization direction as indicated by the arrow: since the tip is pointing either parallel (left) or perpendicular (right) to the rotation plane of the spin spiral, the magnetic signal is maximized on the left domain and minimized on the other. To obtain the black lines of Fig. 1(i) the simulations have to be performed at the same values for a P and γ as in (e) and (d) for the left and right domain, respectively.[21]

We now demonstrate that more complex magnetic states can also give rise to a TAMR signal by turning to the transverse conical spin spiral structure which occurs in a Mn double-layer on W(110), see Fig. 2(a).[22] This spin spiral propagates along the [001]-direction of the surface with a wavelength of $\lambda_\mathrm{M} \approx 2.4$ nm. It is characterized by continuously varying [110]- and [001]-magnetization components and a constant absolute value of the magnetization projection onto $[1\bar{1}0]$. Measurements of this spin spiral with an out-of-plane magnetized tip, Fig. 2(b) and 2(c), lead to a characteristic pattern of bright and dark stripes, similar to Fig. 1(e). Due to the opposite magnetization directions of the tip these two measurements at the same sample position show a phase shift of $\lambda_\mathrm{M}/2$ for the magnetic contribution.

To disentangle the spin-polarized signal from the structural and electronic contributions, we analyze the difference and the sum of the images: while the first [Fig. 2(d)] shows the magnetic period λ_M, the latter represents the modulation due to the TAMR [Fig. 2(e)]. As in the previous example the periods of the two contributions are related by $\lambda_T = \lambda_M/2$

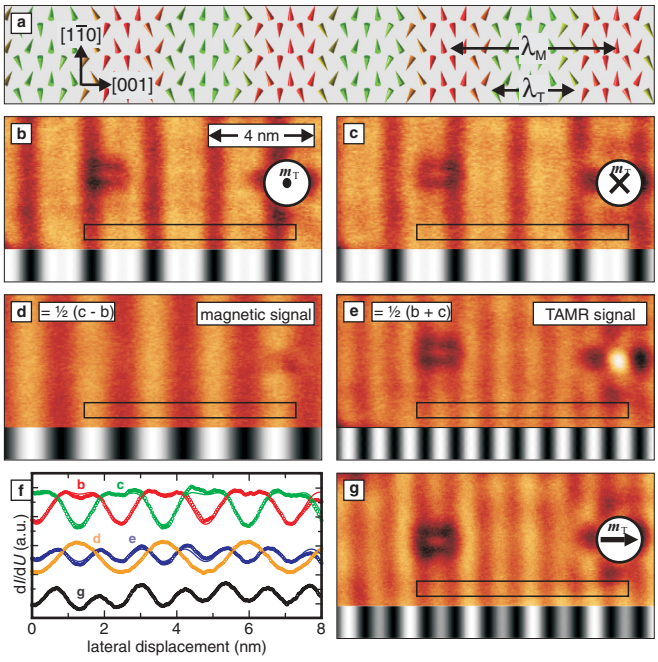

FIG. 2. (Color online) Sketch, spin-polarized STM measurements, and simulations ($P = 0.1$, $\gamma = 0.2$) of the conical spin spiral in the Mn double-layer on W(110).[22] (a) Top view of the magnetic ground state. Red and green symbols indicate positive and negative z components of the magnetization, respectively. (b, c) Spin-polarized $\mathrm{d}I/\mathrm{d}U$ maps of the same sample area imaged with oppositely out-of-plane magnetized tips (spin-polarized tip that aligns with external magnetic field at $B = +2$ T and $B = -2$ T). (d) Difference and (e) sum of images (b) and (c). (f) Line profiles along the indicated boxes and corresponding fits (lines). (g) Spin-polarized $\mathrm{d}I/\mathrm{d}U$ map of the same area with a slightly different, in-plane magnetized tip ($B = 0$ T). All: $I = 1$ nA, $U = -40$ mV, $T = 9$ K.

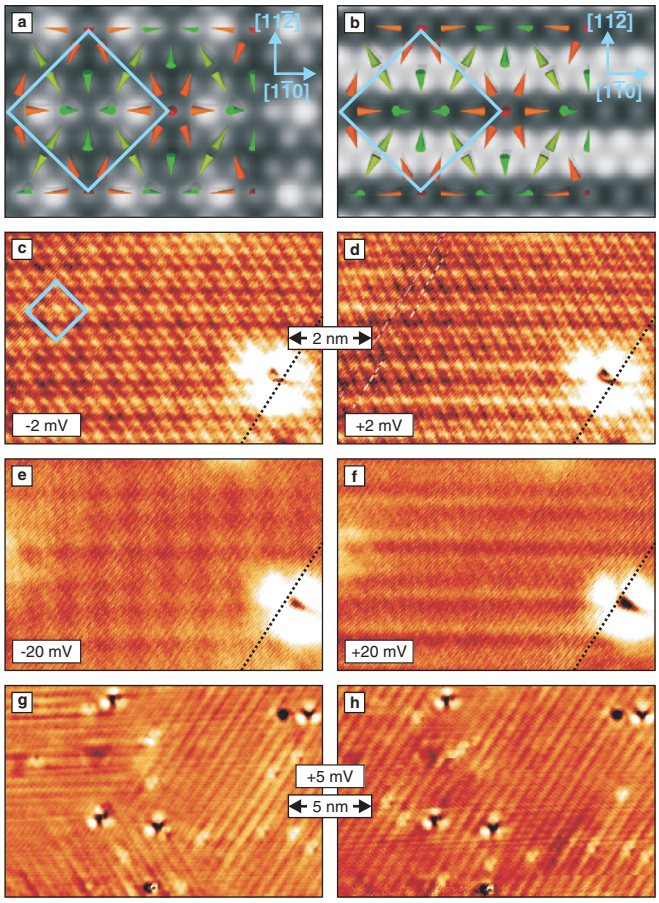

FIG. 3. (Color online) Simulated and measured STM images of a Fe monolayer on a Ir(111) surface. (a, b) Simulated spin-averaged STM images assuming different dependencies of the Fe atoms' LDOS on the direction of their magnetic moment ($P = 0$, $\gamma = 0.1$). The simulations are superimposed with the spin structure of the skyrmion lattice. (c, d) Measured spin-averaged STM images of one rotational domain of the skyrmion lattice and (e, f) STM images of the identical surface area at a higher bias voltage; dotted (black) lines indicate the fast scan axis. (g) Spin-averaged STM image of TAMR patterns of the three rotational domains and (h) the same sample area after the domain structure of the sample was modified. (c–f) $I = 2$ nA, $T = 14$ K; (g, h) $I = 1$ nA, $T = 13$ K.

and compare well with the simulations [Figs. 1(c) and 1(d)]. The signal due to TAMR originates from an LDOS variation with $\cos^2\phi_\alpha$, where ϕ_α is the angle of the spin direction on the cone of the spiral, while the spin-polarized contrast, on the other hand, scales with $\cos(\mathbf{m}_T, \mathbf{m}_\alpha)$. From the scan lines [Fig. 2(f)], we observe that the maxima of the TAMR signal occur between the maxima and the minima in the spin-polarized current. Since we know that the magnetic tip is magnetized perpendicular to the surface we can conclude that, at the chosen bias voltage, TAMR gives rise to a higher $\mathrm{d}I/\mathrm{d}U$ signal for magnetic moments lying in the film plane.

Upon changing the magnetization direction of the tip only the spin-polarized part of the STM image changes while the TAMR contrast is pinned to the spin structure. When performing a measurement with a tip magnetized in the surface plane the STM image shown in Fig. 2(g) is obtained. As expected, the magnetic contrast displays a phase shift of $\pm\lambda_M/4$ compared with the out-of-plane tip [Figs. 2(b) and 2(c)], leading to the observed pattern. The phase shift is also apparent in the line scans presented in Fig. 2(f). For this system the evaluated corrugations of the topography images (not shown) are 1.5 pm for TAMR and also 1.5 pm for the spin-polarized contribution.

The appearance of the TAMR effect becomes more complex when the magnetic structure is two-dimensionally modulated with magnetic moments pointing in all three spatial directions, e.g., the skyrmion lattice of the Fe monolayer on Ir(111)[23] sketched in Figs. 3(a) and 3(b).[24] In this spin structure the projection of the magnetic moments on each of the three spatial coordinates varies, which leads in general to a two-dimensional TAMR pattern. If we assume only mixing of d states with the same spin character, then due to the SOC matrix elements[17] the angular dependence of the LDOS variation $f(\phi_\alpha, \theta_\alpha)$ is $\cos^2\phi_\alpha \sin^2\theta_\alpha$, $\sin^2\phi_\alpha \sin^2\theta_\alpha$, or $\cos^2\theta_\alpha$. Therefore, analogously to the one-dimensional spin states, we expect a unit cell of the TAMR signal which is half the size of the magnetic unit cell. In Figs. 3(a) and 3(b) simulated STM images are shown including an LDOS modulation with the first two dependencies. Such an LDOS modulation can occur, e.g., due to mixing of a d_{z^2} band with a d_{xz} band and a d_{yz} band, respectively. Accordingly, in Fig. 3(a) Fe atoms with large magnetization components along [1$\bar{1}$0] appear brighter

than the other atoms, resulting in a square pattern. Similarly, in Fig. 3(b) atoms with moments mainly pointing along $[11\bar{2}]$ appear brighter, leading to stripes along the diagonal of the magnetic unit cell.

The STM images of the skyrmion lattice in Figs. 3(c)–3(f) demonstrate that, depending on the bias voltage, either one or the other pattern predicted by the model is observed. We attribute this intriguing bias voltage dependence of the TAMR to the fact that STM probes mixing of bands of different orbital characters above and below the Fermi energy. Interestingly, the contributions of atomic corrugation and the electronic TAMR effect can be tuned by slightly increasing the bias voltage, i.e., the tip-sample distance. While in Figs. 3(c) and 3(d) the atomic corrugation is of the same magnitude as the TAMR, the larger bias voltage in Figs. 3(e) and 3(f) leads to pure TAMR images with a corrugation of about 3 pm.

One can exploit the TAMR effect to monitor changes of a noncollinear magnetic structure with non-spin-polarized STM. The STM image in Fig. 3(g) shows the three possible rotational domains of the skyrmion lattice, which can easily be distinguished due to the electronic fingerprint from the TAMR. Figure 3(h) shows a subsequent scan of the same sample area. We observe that due to the voltage pulse between the images, the domain structure changed significantly, as only one rotational domain remains in the image. Of course not only the change in time but also the magnetic phase diagram as a function of T, B, or other parameters can be monitored in this fashion.[25–27] Besides the convenience of using a nonmagnetic tip, this type of measurement has other advantages over spin-polarized STM experiments. While it is sometimes quite tedious to obtain spin-polarized contrast, any nonmagnetic tip which provides high-resolution imaging shows the electronic TAMR effect. In addition, we can exclude a magnetic stray field, which can be a serious problem in experiments using ferromagnetic STM tips.

In conclusion, we have observed the TAMR on the atomic scale in STM experiments for noncollinear spin structures at surfaces. Our experiments demonstrate that the TAMR effect can be scaled down to the ultimate atomic limit, which may be exploited in future spintronic devices.

It is our pleasure to thank Gustav Bihlmayer and Stefan Blügel for insightful discussions. We gratefully acknowledge financial support from the DFG via SFB668, from the ERC Advanced Grant FURORE, and from the Hamburg Cluster of Excellence NANOSPINTRONICS.

*Corresponding author: kbergman@physnet.uni-hamburg.de

[1] C. Gould, C. Rüster, T. Jungwirth, E. Girgis, G. M. Schott, R. Giraud, K. Brunner, G. Schmidt, and L. W. Molenkamp, Phys. Rev. Lett. **93**, 117203 (2004).

[2] J. Moser, A. Matos-Abiague, D. Schuh, W. Wegscheider, J. Fabian, and D. Weiss, Phys. Rev. Lett. **99**, 056601 (2007).

[3] B. G. Park, J. Wunderlich, X. Marti, V. Holý, Y. Kurosaki, M. Yamada, H. Yamamoto, A. Nishide, J. Hayakawa, H. Takahashi *et al.*, Nat. Mater. **10**, 347 (2011).

[4] M. Grünewald, M. Wahler, F. Schumann, M. Michelfeit, C. Gould, R. Schmidt, F. Würthner, G. Schmidt, and L. W. Molenkamp, Phys. Rev. B **84**, 125208 (2011).

[5] S. Mark, L. Ebel, K. Brunner, C. Gould, and L. W. Molenkamp, Appl. Phys. Lett. **99**, 202504 (2011).

[6] S. Mark, P. Dürrenfeld, K. Pappert, L. Ebel, K. Brunner, C. Gould, and L. W. Molenkamp, Phys. Rev. Lett. **106**, 057204 (2011).

[7] J. D. Burton, R. F. Sabirianov, J. P. Velev, O. N. Mryasov, and E. Y. Tsymbal, Phys. Rev. B **76**, 144430 (2007).

[8] D. Jacob, J. Fernández-Rossier, and J. J. Palacios, Phys. Rev. B **77**, 165412 (2008).

[9] K. I. Bolotin, F. Kuemmeth, and D. C. Ralph, Phys. Rev. Lett. **97**, 127202 (2006).

[10] M. Viret, M. Gabureac, F. Ott, C. Fermon, C. Barreteau, G. Autes, and R. Guirado-Lopez, Eur. Phys. J. B **51**, 1 (2006).

[11] J.-M. Tang and M. E. Flatté, Phys. Rev. B **72**, 161315 (2005).

[12] M. Bode, S. Heinze, A. Kubetzka, O. Pietzsch, X. Nie, G. Bihlmayer, S. Blügel, and R. Wiesendanger, Phys. Rev. Lett. **89**, 237205 (2002).

[13] A. Matos-Abiague and J. Fabian, Phys. Rev. B **79**, 155303 (2009).

[14] A. Matos-Abiague, M. Gmitra, and J. Fabian, Phys. Rev. B **80**, 045312 (2009).

[15] C. J. Chen, *Introduction to Scanning Tunneling Microscopy* (Oxford University Press, New York, 1993).

[16] S. Heinze, Appl. Phys. A **85**, 407 (2006).

[17] E. Abate and M. Adsente, Phys. Rev. **140**, A1303 (1965).

[18] From a previous experiment on the domain pattern of Fe/W(110) and first-principles calculations,[12] we can estimate γ to be of the order of 0.1. However, SOC modifies the electronic structure in a way characteristic for a particular system and the actual value of γ will depend on the system and on the bias voltage.

[19] P. Ferriani, K. von Bergmann, E. Y. Vedmedenko, S. Heinze, M. Bode, M. Heide, G. Bihlmayer, S. Blügel, and R. Wiesendanger, Phys. Rev. Lett. **101**, 027201 (2008).

[20] Using density-functional theory exchange splittings of the order of 3 eV have been found.

[21] The orbital of the tip affects the size of the atomic corrugation.[15] To reproduce the experimental data in Fig. 1(i), we have assumed a d_z^2 tip state and a tip-sample distance of 4 Å. Note that P and γ are not affected by the tip orbital.

[22] Y. Yoshida, S. Schröder, P. Ferriani, D. Serrate, A. Kubetzka, K. von Bergmann, S. Heinze, and R. Wiesendanger, Phys. Rev. Lett. **108**, 087205 (2012).

[23] S. Heinze, K. von Bergmann, M. Menzel, J. Brede, A. Kubetzka, R. Wiesendanger, G. Bihlmayer, and S. Blügel, Nat. Phys. **7**, 713 (2011).

[24] We discuss the commensurate approximation of the skyrmion lattice for simplicity. Based on the STM images it can be shown that the skyrmion lattice is actually incommensurate with the atomic lattice.[23]

[25] E. Y. Vedmedenko, A. Kubetzka, K. von Bergmann, O. Pietzsch, M. Bode, J. Kirschner, H. P. Oepen, and R. Wiesendanger, Phys. Rev. Lett. **92**, 077207 (2004).

[26] M. Bode, M. Heide, K. von Bergmann, P. Ferriani, S. Heinze, G. Bihlmayer, A. Kubetzka, O. Pietzsch, S. Blügel, and R. Wiesendanger, Nature **447**, 190 (2007).

[27] P. Sessi, N. P. Guisinger, J. R. Guest, and M. Bode, Phys. Rev. Lett. **103**, 167201 (2009).